RESEARCH ARTICLE | DECEMBER 19 2025

Influence of Bi surfactant on tetrahedral N interstitial formation and optoelectronic properties of dilute GaAsN alloys

Joshua J. P. Cooper ; Jared W. Mitchell ; Yury Turkulets ; W. M. Linhart ; Or Haim Chaulker ; R. Kudrawiec; Ilan Shalish ; Rachel S. Goldman

Appl. Phys. Lett. 127, 242104 (2025)
https://doi.org/10.1063/5.0304729

Applied Physics Letters ARTICLE pubs.aip.org/aip/apl

Influence of Bi surfactant on tetrahedral N interstitial formation and optoelectronic properties of dilute GaAsN alloys

Cite as: Appl. Phys. Lett. **127**, 242104 (2025); doi: 10.1063/5.0304729
Submitted: 30 September 2025 · Accepted: 26 November 2025 ·
Published Online: 19 December 2025

Joshua J. P. Cooper,[1] Jared W. Mitchell,[2] Yury Turkulets,[1] W. M. Linhart,[3] Or Haim Chaulker,[4] R. Kudrawiec,[3] Ilan Shalish,[4] and Rachel S. Goldman[1,2,a)]

AFFILIATIONS

[1]Department of Materials Science and Engineering, University of Michigan, Ann Arbor, Michigan 48109, USA
[2]Department of Physics, University of Michigan, Ann Arbor, Michigan 48109, USA
[3]Department of Semiconductor Materials Engineering, Faculty of Fundamental Problems of Technology, Wrocław University of Science and Technology, Wybrzeże Wyspiańskiego 27, 50-370 Wrocław, Poland
[4]Department of Electrical Engineering, Ben Gurion University, Beer Sheva, Israel

[a)]Author to whom correspondence should be addressed: rsgold@umich.edu

ABSTRACT

Dilute nitride semiconductor alloys are attractive for near- to mid-IR optoelectronic applications but their widespread implementation is hindered by efficiency-limiting non-substitutional N incorporation. Although epitaxy in the presence of surfactants has been reported to increase photoluminescence (PL) emission intensity, the impact of surfactants on N incorporation mechanisms and the resulting optoelectronic properties remains unknown. In this work, we examine the influence of a Bi surfactant on non-substitutional N incorporation and the optoelectronic properties of dilute $GaAs_{1-x}N_x$ alloy films. For $GaAs_{1-x}N_x$ alloy films grown with a Bi surfactant, tetrahedral N interstitial (N_{tetra}) formation is suppressed while the near-band edge PL emission intensity is increased, deep-level PL emission intensity is decreased, and broadening of the photoreflectance resonance is reduced. We discuss the role of the Bi surfactant-induced surface reconstruction transformation on the suppression of N_{tetra} incorporation, as well as its impact on key optoelectronic properties that are applicable to a variety of highly mismatched alloys.

Dilute nitride semiconductor alloys are attractive for many near- to mid-IR optoelectronic applications; however, their widespread implementation has been hindered by non-substitutional N incorporation that limits optical and transport properties.[1–6] For example, in GaAsN, a non-negligible fraction of N atoms are reported to incorporate non-substitutionally as $(N\text{-}N)_{As}$ and/or $(N\text{-}As)_{As}$ split interstitials,[6–9] with tetrahedral N interstitials, N_{tetra}, observed above a threshold N composition,[10] which is dependent on heterovalent doping.[11]

For dilute nitride semiconductors, epitaxy in the presence of surfactants, such as Bi, is reported to reduce surface roughness[12–14] and increase N incorporation,[9,12] while reducing dopant activation[14] and enhancing photoluminescence (PL) emission intensity.[12] In the case of $GaAs_{1-x}N_x$ alloys, a Bi surfactant-induced increase in N concentration has been attributed in part to enhanced non-substitutional N incorporation.[9] Furthermore, a Bi surfactant-induced long-range chemical ordering in $GaAs_{1-x}N_x$ alloys has been attributed to Bi-enhanced alignment of dimer rows along the [110] direction.[15] However, to date, the influence of a Bi surfactant on N_{tetra} incorporation and the resulting optoelectronic properties of GaAsN alloys has yet to be reported.

Here, we examine the influence of a Bi surfactant on non-substitutional N incorporation and the optoelectronic properties of dilute $GaAs_{1-x}N_x$ alloy films. Reflection high-energy electron diffraction (RHEED) reveals a Bi surfactant-induced transformation of the growth surface from a (2×1) to a (3×1) reconstruction. The resulting increase in the ratio of A-type to B-type step edges enhances the incorporation of N into split interstitials, $(N\text{-}N)_{As}$ or $(N\text{-}As)_{As}$ while suppressing their incorporation as N_{tetra}. For both $GaAs_{1-x}N_x$ and $GaAs_{1-x}N_x$:Bi films, photocurrent spectra reveal transitions associated with the GaAs and GaAsN bandgaps, along with a deep level likely within the GaAsN bandgap. However, in the presence of the Bi surfactant, the near-band edge PL emission intensity is increased, the deep-level PL emission intensity is decreased, and broadening of the

photoreflectance resonance is reduced. We discuss the direct links between surfactant-mediated epitaxy, N_{tetra} incorporation, and key optoelectronic parameters, which are applicable to a variety of highly mismatched alloys.

For these investigations, epitaxial GaAsN and GaAsN:Bi films on semi-insulating GaAs (001) substrates were prepared by molecular-beam epitaxy (MBE), using $\geq$ 99.99999 % pure Ga and As and $\geq$ 99.9999 % pure Bi. In addition, N plasma was generated in an Addon RF source operating at high brightness mode (350 W) using $\geq$ 99.9999 % pure N_2 flowing at 0.25 sccm. The targeted layer thicknesses were determined using growth rate calibrations based upon reflection high-energy electron diffraction (RHEED) oscillations. Following oxide desorption and growth of a $\sim$500 nm thick GaAs buffer layer at 580 °C, the substrate temperature was lowered to 395 $\pm$ 15° and the samples were annealed for 5–10 min to achieve a flat buffer. Subsequently, 450 $\pm$ 50 nm thick GaAsN:Bi films were grown at a rate of 1.0 μm/h, with and without a Bi flux of 8.0×10^{-9} Torr.

To monitor the influence of the Bi flux on the surface reconstruction, RHEED patterns were collected during epitaxy [Figs. 1(a)–1(d)]. During GaAsN growth, the surface transforms from the GaAs (2 × 4) to the GaAsN (2 × 1) reconstruction [Fig. 1(e)], expected to consist primarily of [1 $\bar{1}$ 0]-aligned (A-type) step edges.[16] In the presence of a Bi surfactant, shown in Fig. 1(f), the surface reconstruction further transforms to GaAsN:Bi (1 × 3), expected to increase the ratio of [110]-aligned (B-type) to [1 $\bar{1}$ 0]-aligned (A-type) step edges.[16,17] For the A-type step edges in Fig. 1(g), Ga dangling bonds provide opportunities for Ga-N bond formation, allowing the formation of N_{As} or N_{tetra}. On the other hand, for the B-type step edges in Fig. 1(h), arsenic dangling bonds facilitate the formation of $(N\text{-}As)_{As}$.[9]

For both films, the surface morphology was probed using tapping mode atomic-force microscopy (Veeco Dimension Icon in ScanAsyst mode) and scanning electron microscopy (LEO-A Zeiss 982 FEG-SEM). High-resolution x-ray rocking curves were generated using Cu-Kα_1 radiation (Bede D1), with $\Delta\omega$ scans collected near the GaAs (004) and (224) reflections, as described elsewhere.[18,19] Assuming tensile-strained GaAsN films, the residual coherency strains were determined using a linear interpolation of binary elastic constants and lattice parameters for zinc blende GaAs and GaN,[20,21] along with NRA-determined N compositions, $x_N = 0.015 \pm 0.003$.

Simultaneous NRA and RBS measurements were conducted using 4.5 MeV α ions generated in a 1.7 MV General Ionex tandem ion accelerator, with backscattered α ions and proton yields from $^{14}N(\alpha,p)^{17}O$ detected by silicon (Si) surface-barrier detectors

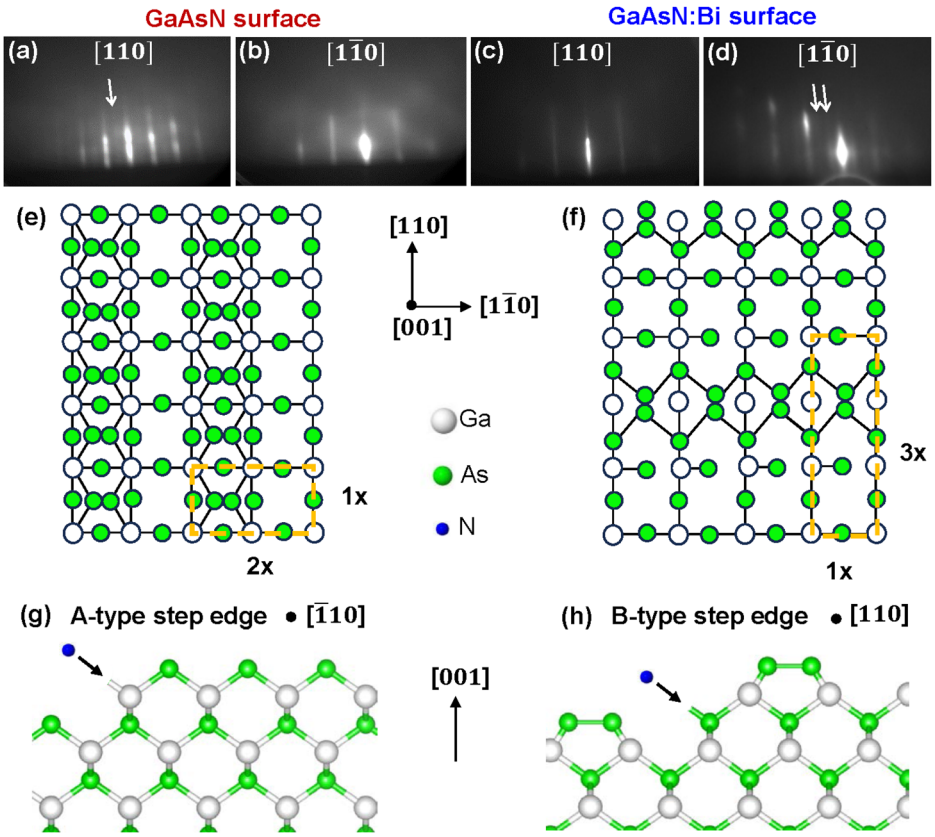

FIG. 1. Surface reconstructions and corresponding atomic models: (a) Reflection high-energy electron diffraction patterns for GaAsN [(a) and (b)] and GaAsN:Bi [(c) and (d)], with downward-pointing arrows indicating the higher order 2 × and 3 × reflections in (a) and (d). During GaAsN growth, the (c) (2 × 1) reconstruction is expected to contain a high density of (e) A-type step edges, with Ga dangling bonds that enable substitutional N (N_{As}) or tetrahedral N interstitial (N_{tetra}) formation. The (d) Bi-induced (1 × 3) surface reconstruction is expected to contain a high density of (f) B-type step edges, with arsenic dangling bonds that facilitate the formation of $(N\text{-}As)_{As}$ split interstitial complexes.[9]

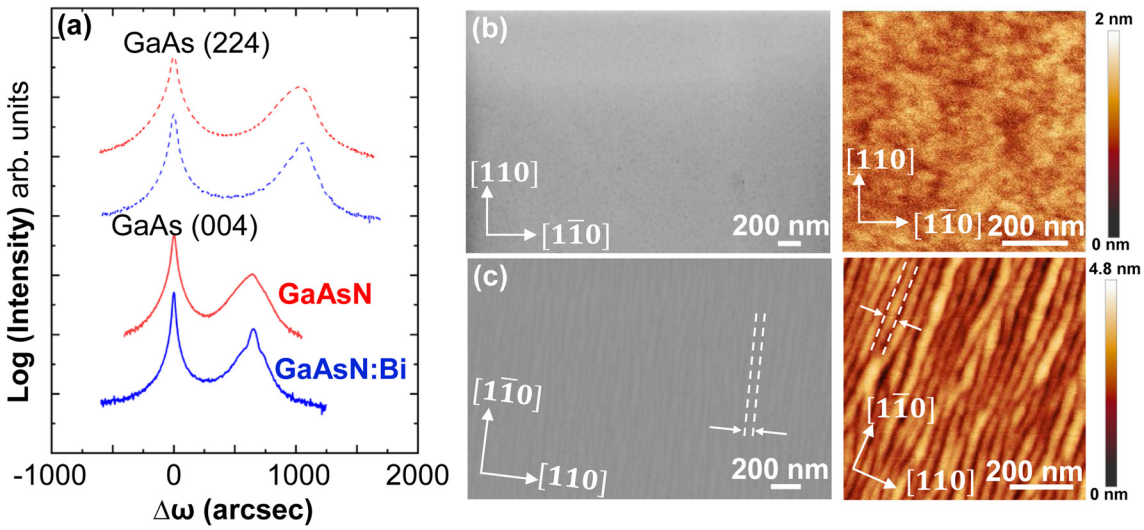

FIG. 2. GaAsN:Bi film composition and morphology: (a) High-resolution $\Delta\omega$ scans about the (004) and (224) GaAs for the GaAsN (red) and GaAsN:Bi (blue) films. Analysis of the $\Delta\omega_{(004)}$ and $\Delta\omega_{(224)}$ data reveals residual tensile strains of $0.22 \pm 0.01\%$. Scanning electron micrographs and corresponding atomic-force micrographs of the surfaces of (b) GaAsN and (c) GaAsN:Bi films, with color-scale ranges, Δ z, of (b) 2.0 and (c) 4.8 nm. For the (c) GaAsN:Bi films, 50-nm-wide surface mounds aligned along the [1 $\bar{1}$ 0] are identified in the SEM and AFM images of the GaAsN:Bi surface.

positioned at 170° and 135° relative to the incident beam. RBS and NRA yields vs particle energy were measured in the [100], [110], and [111] channels, as well as in random (non-channeling) conditions, achieved with $\phi = 5°$ away from the channel and rotating the specimen $\pm 5°$ in θ by steps of 0.2°.[10] For each film, the ratio of the channeling to random yields, summed over the top 400 nm, was used to determine the minimum RBS and NRA yields, $\chi_{min,GaAs}$ and $\chi_{min,N}$. Using the 5-axis goniometer, the angular dependence of RBS and NRA yields (so-called "angular yield scans") wase measured at $\pm$ 1.5° in steps of 0.1° about $\langle 110 \rangle$ rotation axes, in the [100], [111], and [110] channeling directions. Please see the supplementary material for more details on the channeling ion beam analysis.

Following deposition of Ti/Pt/Au (7/20/50 nm) contacts using electron-beam evaporation, room temperature photocurrent spectra were measured as a function of illumination wavelength using a Keithley 2400 current source with 5 V applied voltage. Sample illumination was achieved using a 300 W Xe short-arc lamp monochromated by a Newport MS257 spectrometer and filtered by order-sorting filters. A fixed photon flux was maintained using a computer-controlled slit, and the dark current was subtracted from the data. PR spectra were measured at 20 K using a 532 nm semiconductor laser and a 150 W tungsten–halogen bulb as the pump and probe beam, respectively. Finally, PL spectra were collected at 20 K using a 532 nm continuous-wave laser at an excitation power of 100 (or 300) mW.

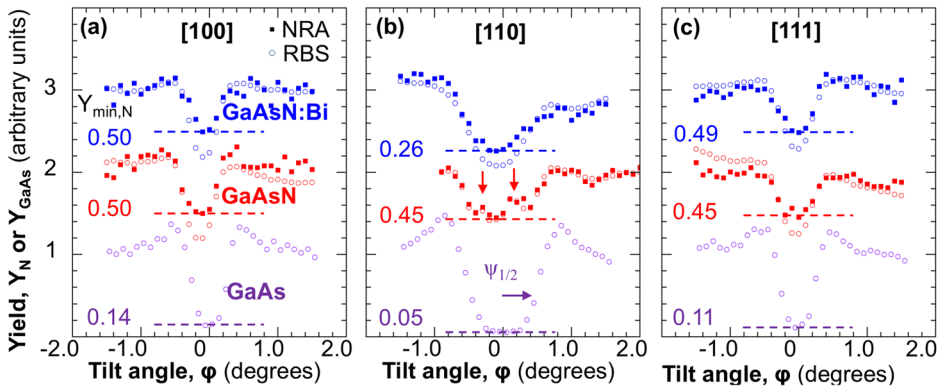

FIG. 3. Angular yield scans collected from the top 400 nm of GaAs (purple), GaAsN (red), and GaAsN:Bi (blue) films: The plots display the backscattered yield (RBS), Y_{GaAs} (open circles), and $^{14}N(\alpha,p)^{17}O$ yield (NRA), Y_N (filled squares), vs tilt angle in ϕ about a $\langle 110 \rangle$ rotation axis for each of the (a) [100], (b) [110], and (c) [111] channeling directions. For each angular yield scan, dashed horizontal lines mark the minimum yields, $Y_{min,GaAs}$ (GaAs) and $Y_{min,N}$ (GaAsN and GaAsN:Bi), and horizontal arrows mark the half-width at half depth, $\Psi_{1/2,GaAs}$. For all channeling directions, well-defined channels, with $Y_{min,GaAs} \leq 0.14$, are observed for the GaAs reference. For the (a) [100] and (c) [111] channeling directions, well-defined channels and similar $Y_{min,GaAs}$ and $Y_{min,N}$ values are observed for both GaAsN and GaAsN:Bi. For the (b) [110] channel, well-defined channels are apparent for GaAsN:Bi, but increased Y_N and flux peaking features near $\phi = \pm 0.3°$ for the GaAsN film reveal the presence of tetrahedral N interstitials (N_{tetra}).

Figure 2(a) shows a series of high-resolution $\Delta\omega$ scans about (004) GaAs and (224) GaAs for the GaAsN (red) and GaAsN:Bi (blue) films, along with AFM and SEM images collected from the GaAsN [Fig. 2(b)] and GaAsN:Bi [Fig. 2(c)] films. In Fig. 2(a), the GaAs substrate peak is set to $\Delta\omega = 0$ arcsec, leading to $\Delta\omega_{(004)} = \sim 639 \pm 11$ arcsec and $\Delta\omega_{(224)} = \sim 1034 \pm 20$ arcsec for both the GaAsN and GaAsN:Bi films. Analysis of the $\Delta\omega_{(004)}$ and $\Delta\omega_{(224)}$ data reveals residual tensile strains of $0.22 \pm 0.01\%$. For the GaAsN film, the corresponding AFM and SEM micrographs [Fig. 2(b)] reveal smooth, featureless surfaces, with height variation ≤ 0.2 nm. The residual strain and surface roughness are similar to reported values for MBE-grown GaAsN films.[18] On the other hand, for the GaAsN:Bi film [Fig. 2(c)], $[1\bar{1}0]$-aligned surface "mounds" (~ 4.3 nm height, ~ 50 nm width) are apparent, similar to an earlier report.[15]

We now consider the measured minimum yields from RBS and NRA, provided in the supplemental materials. For the GaAs reference, $\chi_{min,GaAs} \sim 0.05$. Similarly, for GaAsN:Bi, $\chi_{min,GaAs} \sim 0.10 \pm 0.04$, indicating minimal displacement of Ga and As atoms from lattice positions. In addition, for GaAsN:Bi, $\chi_{min,N} \sim 0.29 \pm 0.05$, suggesting that $71 \pm 5\%$ of the N has incorporated substitutionally. On the other hand, for GaAsN grown without a Bi flux, $\chi_{min,GaAs} = 0.015 \pm 0.07$ and $\chi_{min,N} \sim 0.36 \pm 0.12$ in the [100] and [111] channels, with a significant increase in $\chi_{\mathrm{min,GaAs}}$ and $\chi_{\mathrm{min,N}}$ in the [110] channeling direction, indicating displacement of N and Ga and/or As atoms into the [110] channel. This observation is consistent with the presence of both N_{tetra} as well as Ga and/or As tetrahedral interstitials.[10,22,23]

To determine the impact of the Bi surfactant on atomic displacements into the channels, we consider the angular yield scans in Figs. 3(a)–3(c): Y_{GaAs} (open circles) and Y_N (filled squares) as a function of tilt angle, ϕ, about a $\langle 110 \rangle$ rotation axis, for the GaAs (purple), GaAsN (red), and GaAsN:Bi (blue) films. For GaAs, a minimum in $Y_{GaAs}(\phi)$, $Y_{\mathrm{min,GaAs}}$, is observed at 0° where the incident ion beam is aligned along the [100] [Fig. 3(a)], [110] [Fig. 3(b)], and [111] [Fig. 3(c)] directions. For each angular yield scan in Fig. 3, the minimum in $Y_N(\phi)$, $Y_{\mathrm{min,N}}$, is illustrated by dashed horizontal lines; the half-width at half depth, $\Psi_{1/2,GaAs}$, is denoted by the horizontal arrow in Fig. 3(b).

For the [100] and [111] channels [Figs. 3(a) and 3(c)], $Y_{\mathrm{min,GaAs}}$, $Y_{\mathrm{min,N}}$, $\Psi_{1/2,GaAs}$, and $\Psi_{1/2,N}$ are similar for the GaAsN and GaAsN:Bi films. On the other hand, for both the GaAsN and GaAsN:Bi, $Y_{\mathrm{min,N}} > Y_{\mathrm{min,GaAs}}$ of the reference GaAs film,[10] suggesting the presence of $(\mathrm{N\text{-}N})_{As}$ and $(\mathrm{N\text{-}As})_{As}$. For the [110] channel [Fig. 3(b)], significant increases in $Y_{\mathrm{min,GaAs}}$ and $Y_{\mathrm{min,N}}$ are apparent for the GaAsN layer relative to that of the GaAsN:Bi layer, indicating the displacement of Ga and/or As, as well as N atoms into the [110] channel. For the GaAsN film, increases in Y_{GaAs} and Y_N within the channel, often termed "flux peaking" features, are denoted by a downward-pointing arrow at $\pm 0.3°$ [Fig. 3(b)], indicating the presence of tetrahedral interstitials.[24]

We now discuss the optoelectronic properties of the GaAsN films. Figure 4(a) shows room temperature photoconductivity spectra collected from the GaAsN and GaAsN:Bi films. Transitions at 1.2 and 1.4 eV are attributed to GaAsN:Bi and GaAs bandgaps, respectively, with the broad peak at 0.85 eV likely due to a deep level in GaAsN. Figures 4(b) and 4(c) show PR and PL spectra collected at 20 K. For the PR data in Fig. 4(b), the energy and broadening of the resonances were obtained with an Aspnes fit. For both GaAsN and GaAsN:Bi, strong resonances at 1.29 eV are apparent. The 70 meV difference in emission and absorption "bandgaps," or Stokes shift, suggests emission from localized states within the bandgap. Interestingly, the broadening parameter is reduced from 26.5 meV for GaAsN to 13 meV for GaAsN:Bi, suggesting that Bi has passivated the N-related non-radiative recombination centers.

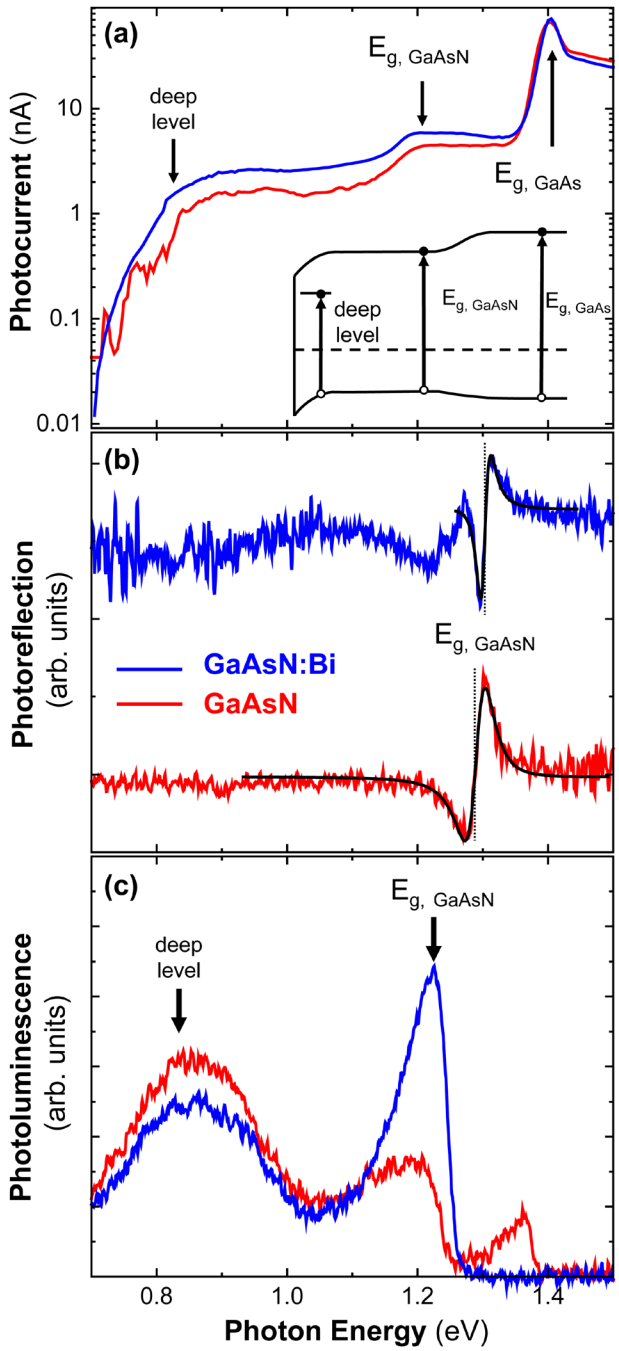

FIG. 4. Optoelectronic properties of GaAsN (red) and GaAsN:Bi (blue) films: (a) Photocurrent (room temperature), (b) photoreflectance (20 K), and (c) photoluminescence (20 K) spectra. Features associated with the GaAs and GaAsN bandgaps as well as a deep level in GaAsN are labeled in each plot.

For the PL data in Fig. 4(c), a broad low-energy emission at 0.85 eV, a wide dip at 1.05 eV, and a sharp emission at 1.22 eV are observed for both GaAsN and GaAsN:Bi. The low-energy emission may be due to deep levels associated with As_{Ga}, often reported in GaAs grown at low temperatures,[25–27] or to the presence of N-related deep levels.[27–30] Interestingly, the intensity of the low-energy emission is reduced in GaAsN:Bi, presumably due to passivation of N-related deep levels. Meanwhile, the sharp emission at 1.22 eV, which is more intense in GaAsN:Bi, is likely due to near-band edge recombination of localized excitons.

In summary, we report on the effect of a Bi surfactant on N incorporation mechanisms and the optoelectronic properties of GaAsN films. During GaAsN epitaxy, the Bi surfactant induces a transformation of the surface reconstruction, leading to an increase in the ratio of B-type to A-type step edges that enhances the incorporation of N into split interstitials, $(N\text{-}N)_{As}$ or $(N\text{-}A)_{As}$, while suppressing the formation of tetrahedral N interstitials, N_{tetra}. The Bi surfactant-induced reduction in N_{tetra} incorporation into GaAsN occurs simultaneously with improvements in the PL emission efficiency. Thus, this study demonstrates the key role of surfactants in suppressing the formation of N_{tetra} in order to enhance the optoelectronic properties of GaAsN. This approach is likely to be applicable to a variety of highly mismatched semiconductor alloys, especially those containing dilute concentrations of N.

See the supplementary material for a description of channeling ion beam analysis, as well as the RBS and NRA yield vs energy spectra and the resulting RBS and NRA χ_{min} values in the [100], [110], and [111] channeling directions.

We gratefully acknowledge receiving support from the National Science Foundation (Grant Nos. ECCS 2240388 and DMR 1810280), the Department of Energy (Grant No. DE-SC0023222), and the United States–Israel Binational Science Foundation (2022627).

AUTHOR DECLARATIONS

Conflict of Interest

The authors have no conflicts to disclose.

Author Contributions

Joshua J. P. Cooper: Conceptualization (equal); Data curation (equal); Formal analysis (equal); Investigation (equal); Methodology (equal); Resources (equal); Validation (equal); Writing – original draft (equal); Writing – review & editing (equal). **Jared W. Mitchell:** Conceptualization (equal); Data curation (equal); Formal analysis (equal); Investigation (equal); Methodology (equal); Resources (equal); Validation (equal); Writing – original draft (equal); Writing – review & editing (equal). **Yury Turkulets:** Data curation (equal); Formal analysis (equal); Investigation (equal); Methodology (equal); Resources (equal); Validation (equal); Writing – original draft (equal); Writing – review & editing (equal). **W. M. Linhart:** Data curation (equal); Investigation (equal); Methodology (equal); Resources (equal); Validation (equal); Writing – review & editing (supporting). **Or Haim Chaulker:** Data curation (equal); Formal analysis (equal); Investigation (equal); Methodology (equal); Validation (equal); Writing – review & editing (supporting). **R. Kudrawiec:** Data curation (equal); Formal analysis (equal); Methodology (equal); Resources (equal); Writing – review & editing (supporting). **Ilan Shalish:** Data curation (equal); Formal analysis (equal); Methodology (equal); Resources (equal); Writing – review & editing (equal). **Rachel S. Goldman:** Conceptualization (equal); Formal analysis (equal); Funding acquisition (lead); Methodology (equal); Project administration (lead); Resources (lead); Supervision (lead); Validation (equal); Writing – review & editing (lead).

DATA AVAILABILITY

The data that support the findings of this study are available within the article and its supplementary material.

REFERENCES

[1]Y. Jin, R. M. Jock, H. Cheng, Y. He, A. M. Mintarov, Y. Wang, C. Kurdak, J. L. Merz, and R. S. Goldman, "Influence of N interstitials on the electronic properties of GaAsN alloys," Appl. Phys. Lett. **95**, 062109 (2009).
[2]K. Yamane, Y. Maki, S. One, A. Wakahara, E.-M. Pavelescu, T. Ohshima, T. Nakamura, and M. Imaizumi, "Mechanism of improved crystallinity by defect-modification in proton-irradiated GaAsPN photovoltaics: Experimental and first-principle calculations approach," J. Appl. Phys. **132**, 065701 (2022).
[3]H. Kawata, S. Hasegawa, J. Matsumura, H. Nishinaka, and M. Yoshimoto, "Fabrication of a GaAs/GaNAsBi solar cell and its performance improvement by thermal annealing," Semicond. Sci. Technol. **36**, 095020 (2021).
[4]S. Fahy, A. Lindsay, H. Ouerdane, and E. P. O'Reilly, "Alloy scattering of n-type carriers in GaN_xAs_{1-x}," Phys. Rev. B **74**, 035203 (2006).
[5]E.-M. Pavelescu, O. Ligor, J. Occena, C. Ticoş, A. Matei, R. L. Gavrilă, K. Yamane, A. Wakahara, and R. S. Goldman, "Influence of electron irradiation and rapid thermal annealing on photoluminescence from GaAsNBi alloys," Appl. Phys. Lett. **117**, 142106 (2020).
[6]F. Ishikawa, S. Fuyuno, K. Higashi, M. Kondow, M. Machida, H. Oji, J.-Y. Son, A. Trampert, K. Umeno, Y. Furukawa, and A. Wakahara, "Direct observation of N-(group V) bonding defects in dilute nitride semiconductors using hard x-ray photoelectron spectroscopy," Appl. Phys. Lett. **98**, 121915 (2011).
[7]T. Jen, G. Vardar, Y. Q. Wang, and R. S. Goldman, "Identifying the dominant interstitial complex in dilute GaAsN alloys," Appl. Phys. Lett. **107**, 221904 (2015).
[8]M. C. López-Escalante, B. Ściana, W. Dawidowski, K. Bielak, and M. Gabás, "Atomic configurations in AP-MOVPE grown lattice-mismatched InGaAsN films unravelled by X-ray photoelectron spectroscopy combined with bulk and surface characterization techniques," Appl. Surf. Sci. **433**, 1–9 (2018).
[9]J. Occena, T. Jen, E. E. Rizzi, T. M. Johnson, J. Horwath, Y. Q. Wang, and R. S. Goldman, "Bi-enhanced N incorporation in GaAsNBi alloys," Appl. Phys. Lett. **110**, 242102 (2017).
[10]J. J. P. Cooper, T. Jen, A. Novak, Z. Xi, L. Qi, F. U. Naab, Y. Q. Wang, and R. S. Goldman, "Onset of tetrahedral interstitial formation in GaAsN alloys," Appl. Phys. Lett. **124**, 161108 (2024).
[11]J. J. P. Cooper, M. C. Carcassi, Z. Xi, D. J. Womack, H. D. L. McKenna, L. Qi, and R. S. Goldman, "Influence of heterovalent doping on tetrahedral N interstitial formation in dilute GaAsN alloys," Appl. Phys. Lett **127**, 202102 (2025).
[12]S. Tixier, M. Adamcyk, E. C. Young, J. H. Schmid, and T. Tiedje, "Surfactant enhanced growth of GaNAs and InGaNAs using bismuth," J. Cryst. Growth **251**, 449–454 (2003).
[13]E. C. Young, S. Tixier, and T. Tiedje, "Bismuth surfactant growth of the dilute nitride GaN_xAs_{1-x}," J. Cryst. Growth **279**, 316–320 (2005).
[14]T. Liu, S. Chandril, A. J. Ptak, D. Korakakis, and T. H. Myers, "Bismuth surfactant effects for GaAsN and beryllium doping of GaAsN and GaInAsN grown by molecular beam epitaxy," J. Cryst. Growth **304**, 402 (2007).
[15]J. Occena, T. Jen, H. Lu, B. A. Carter, T. S. Jimson, A. G. Norman, and R. S. Goldman, "Surfactant-induced chemical ordering of GaAsN:Bi," Appl. Phys. Lett. **113**, 211602 (2018).
[16]A. Duzik, J. C. Thomas, J. M. Millunchick, J. Lång, M. P. J. Punkkinen, and P. Laukkanen, "Surface structure of bismuth terminated GaAs surfaces grown with molecular beam epitaxy," Surf. Sci. **606**, 1203–1207 (2012).
[17]M. D. Pashley, K. W. Haberern, and J. M. Gaines, "Scanning tunneling microscopy comparison of GaAs(001) vicinal surfaces grown by molecular beam epitaxy," Appl. Phys. Lett. **58**, 406 (1991).

[18]M. Reason, N. G. Rudawski, H. A. McKay, X. Weng, W. Ye, and R. S. Goldman, "Mechanisms of GaAsN growth: Surface and step-edge diffusion," J. Appl. Phys. **101**, 083520 (2007).
[19]J. Occena, T. Jen, J. W. Mitchell, W. M. Linhart, E.-M. Pavelescu, R. Kudrawiec, Y. Q. Wang, and R. S. Goldman, "Mapping the composition-dependence of the energy bandgap of GaAsNBi alloys," Appl. Phys. Lett. **115**, 082106 (2019).
[20]K. Kim, W. R. L. Lambrecht, and B. Segall, "Elastic constants and related properties of tetrahedrally bonded BN, AlN, GaN, and InN," Phys. Rev. B **53**, 16310 (1996).
[21]J. S. Blakemore, "Semiconducting and other major properties of gallium arsenide," J. Appl. Phys. **53**, R123 (1982).
[22]J. Nakata, M. Taniguchi, and K. Takahei, "Direct evidence of Er atoms occupying an interstitial site in metalorganic chemical vapor deposition-grown GaAs:Er," Appl. Phys. Lett. **61**, 2665 (1992).
[23]H. Kobayashi, K. Kimura, F. Nishiyama, S. Miwa, and T. Yao, "Lattice location of N in ZnSe by channeling-NRA," Nucl. Instrum. Methods B **132**, 142 (1997).
[24]H. Krause, M. Lux, E. Nowak, J. Vogt, R. Flagmeyer, G. Kühn, and G. Otto, "Lattice site localization of Zn in InP using the PIXE/channeling technique," Phys. Status Solidi A **132**, 295 (1992).
[25]K. Yu, M. Kaminska, and Z. Liliental-Weber, "Characterization of GaAs layers grown by low temperature molecular beam epitaxy using ion beam techniques," J. Appl. Phys. **72**, 2850 (1992).
[26]M. Kaminska and E. R. Weber, "Low temperature GaAs: Electrical and optical properties," Mater. Sci. Forum **83–87**, 1033 (1992).
[27]S. B. Zhang and S.-H. Wei, "Nitrogen solubility and induced defect complexes in epitaxial GaAs:N," Phys. Rev. Lett. **86**, 1789 (2001).
[28]D. Sentosa, T. Xiaohong, and C. Jin, "Luminescence from the deep level N–N interstitials in GaAsN grown by metal organic chemical vapour deposition," CrystEngComm **12**, 2153 (2010).
[29]Ł. Gelczuk, H. Stokowski, M. Dąbrowska-Szata, and R. Kudrawiec, "Origin and annealing of deep-level defects in GaNAs grown by metalorganic vapor phase epitaxy," J. Appl. Phys. **119**, 185706 (2016).
[30]R. Kudrawiec, M. Latkowska, M. Welna, J. Misiewicz, M. Shafi, R. Mari, M. Henini, and W. Walukiewicz, "Correlations between the band structure, activation energies of electron traps, and photoluminescence in n-type GaNAs layers," Appl. Phys. Lett. **101**, 082109 (2012).